The anti-inflammatory peptide Catestatin blocks chemotaxis

Elke M. Muntjewerff[1], Kristel Parv[2], Sushil K. Mahata[3,4], Mia Phillipson[2,5], Gustaf Christoffersson[2,5*], Geert van den Bogaart[1,6*]

[1] Department of Tumor Immunology, Radboud Institute for Molecular Life Sciences, Radboud University Medical Center, Nijmegen, the Netherlands

[2] Department of Medical Cell biology, Uppsala University, Uppsala, Sweden

[3] VA San Diego Healthcare System and

[4] Department of Medicine, University of California San Diego, La Jolla, California, USA

[5] Science for Life Laboratory, Uppsala University, Uppsala, Sweden

[6] Department of Molecular Immunology and Microbiology, Groningen Biomolecular Sciences and Biotechnology Institute, University of Groningen, Groningen, the Netherlands.

*** Correspondence:**

Geert van den Bogaart: g.van.den.bogaart@rug.nl

Gustaf Christoffersson: gustaf.christoffersson@scilifelab.uu.se

Keywords: Catestatin$_1$, Macrophages$_2$, Monocytes$_3$, Pro-angiogenesis$_4$, Granulocytes$_5$, Chemotaxis$_6$, Migration$_7$

Word count: 1.468
Figures: 2

Abstract

Increased levels of the anti-inflammatory peptide catestatin (CST), a cleavage product of the pro-hormone chromogranin A, correlates with less severe outcomes in hypertension, colitis and diabetes. However, it is unknown how CST reduces the infiltration of monocytes and macrophages in inflamed tissues. Here, we report that CST blocks leukocyte migration towards inflammatory chemokines. By *in vitro* and *in vivo* migration assays, we show that although CST itself is weakly chemotactic, it blocks migration of monocytes and granulocytes to inflammatory attracting factor CC-chemokine ligand 2 (CCL2) and macrophage inflammatory protein 2 (MIP-2). Moreover, it directs CX_3CR1^+ macrophages away from pancreatic islets. These findings support the emerging notion that CST is a key anti-inflammatory modulator.

1. Introduction

As an immunological response to inflammation, monocytes, granulocytes and leukocytes are attracted to inflamed tissues by chemokines such as CC-chemokine ligand 2 (CCL2, a.k.a. MCP-1) and macrophage inflammatory protein 2 (MIP-2, a.k.a. CXCL2) (1). However, to avoid an excessive response, leukocyte infiltration should be halted for resolution of inflammation, but the mechanisms that govern this are unknown (2). Here, we addressed the potential chemotactic effect of chromogranin A (CgA)-derived peptide Catestatin (CST: $hCgA_{352-372}$) (3). While CST circulates at low nM range, the local concentrations were detected in the µM range in mouse tissues (3–6).

Being an anti-inflammatory peptide, CST reduces inflammation in cardiac and chronic inflammatory diseases (3,7–9). Despite the chemotactic effects of CST (7,10,11), administration of exogenous CST reduces monocyte and macrophage infiltration in the liver, heart and gut in mouse models of type II diabetes, hypertension, atherosclerosis and colitis (4,7,8,12,13). In a colitis model, CST also reduced granulocyte infiltration in the colon (8). In line with this, the adrenal gland, heart, and gut of CST knockout mice display increased macrophage infiltration (4,7,12). In this study, we show that while CST itself is weakly chemotactic, it blocks the extravasation and migration of phagocytes both *in vitro* and *in vivo.* Thus, the anti-inflammatory effects of CST are partly the result of redirecting monocytes and granulocytes away from the inflammation sites.

2. Methods; experimental procedures

2.1 Animals and human bloods samples

Male and female C57BL/6J (Taconic, Denmark) and *Cx$_3$cr1^{GFP}* (14) mice weighing 20-26 g were used. All animal experiments were approved by the Regional Animal Ethics committee in Uppsala, Sweden. The research with human blood samples at the Department of Tumor Immunology complies with all institutional and national ethics regulations and has been approved by the ethics committee of Sanquin blood bank. All blood donors were informed of the research and have granted their consent.

2.2 Gradientech assay

A CellDirector 2D device (Gradientech) was coated with bovine serum overnight. Human peripheral blood monocytes were isolated from buffy coats of healthy donors as described (15), followed by human microbead CD14$^+$ isolation of monocytes according to manufactures' instructions (130-050-201, Milteny Biotec). Monocytes were activated with LPS for 1 h, washed with PBS, and seeded in the device in 200 µl RPMI-1640 medium. After one hour at 37°C, the two supplied syringes with 1 ml of RPMI-1640 medium, with one containing 5 µM CST were attached to the CellDirector and a flow rate of 5 µl/min was applied. Monocyte movement was visualized with an Axiovert 200 M microscope with a 5x objective (Zeiss, Jena, Germany). Movies were recorded at 2 frames/min for 3 hours. Cell movement was analysed using the Tracking Tool PRO software (Gradientech). 0.5 nM CCL2 (300-04, PeproTech) was used as a positive control.

2.3 Cremaster muscle imaging

Monocyte and granulocyte (Ly6G-mAb) migration was imaged in the cremaster muscle of mice superfused with pre-warmed (37°C) bicarbonate-buffered saline solution (pH 7.4) (16) containing CST (5 µM) and/or MIP-2/CXCL2 (0.5 nM) (250-15, PeproTech) was used as a positive control. A bright-field intravital microscope (Leica DM5000B) with a 25×/0.6W (Leica) objective and connected to an Orca R2 camera (Hamamatsu; Volocity acquisition software) was used to record movies of five minutes at 0, 30, 60, 90 min after cytokine addition. Venules with diameter range of 20-30 µm were imaged. Movies were analysed using ImageJ and corrected using the Hyperstackreg ImageJ macro. For rolling flux, all cells rolling in the vessel were counted. For rolling speed, velocity over a 100 µm section of the vessel was analysed. In the same 100 µm section, cells were considered adherent if they remained stationary for at least 3 min.

2.4 Aortic ring assay with pancreatic islet culture

Aortic ring isolation was carried out as previously described (17). Briefly, 13-16-week-old *Cx$_3$cr1^{GFP}*mice were euthanized, followed by dissection of the thoracic aorta. Under a stereo-microscope, extraneous fat, tissue, and branching vessels were carefully removed,

and perfused with serum-free OptiMEM medium (Thermo Fisher) with penicillin-streptomycin solution. The aorta was sectioned into 1 mm thick rings. After overnight starvation in serum-free Opti-MEM medium, rings were embedded in 1 mg/ml rat tail collagen I (#ALX-522-435-0100, Enzo Life sciences) adjacent to pancreatic islets (2-5 islets per ring), which were isolated from C57BL/6 mice as described before (18), in 8 well Nunc Lab-Tek II microscope chambers (Thermo Fisher). After 1 h, embedded rings were cultured with 300 µl of OptiMEM with 2.5% FBS, 11.1 mM glucose, penicillin-streptomycin, M-CSF (40 ng/ml) to stimulate CX_3CR1^{GFP+} macrophage survival and 5 µM CST for six days. On day six, rings were imaged using a Zeiss LSM700 (Carl Zeiss) confocal microscope. The numbers of CX_3CR1^{GFP+} cells were quantified using the image analysis software Imaris (Bitplane). The location of the CX_3CR1^{GFP+} cells was determined using the Surface Center of Mass Position to Spots object plugin after manually defining the aorta. For analyzing angiogenesis, staining with anti-CD31 antibody conjugated to Alexa Fluor 647 (#102515, Biolegend) was carried out prior to imaging. Aortic rings that did not show any sprouting were excluded from further analysis. Vessels were analyzed using Fiji image analysis software (19). Sprouts that originated directly from the ring endothelium were considered main sprouts, and branches as divarications from main sprouts.

2.5 Statistical data analysis

Data are expressed as mean ± SEM. One-way ANOVA with Bonferroni post-hoc tests or non-parametric Mann-Whitney test were applied for multiple comparisons. Outliers were identified using ROUT test (Q=1%). A value of $p < 0.05$ was considered statistically significant.

3. Results & Discussion

Although human blood monocytes migrated towards a high (but physiological) concentration of CST (5 µM), this was less efficient compared to the canonical inflammatory chemokine CCL2 (0.5 nM) (Fig. 1A-C), reinforcing a weak chemoattractive effect of CST (7,10,11). To confirm this *in vivo*, we performed imaging of the cremaster muscle (Fig. 1D) (16). Upon perfusion of the muscle with CST (5 µM), phagocytes (monocytes and granulocytes) decreased their speed and attached to the vessel wall with similar efficiency as of the inflammatory chemotactic agent MIP-2 (0.5 nM) (Fig. 1D-F, Fig. S1). Thus, both our *in vivo* and *in vitro* migration assays show that CST is weakly chemotactic, raising the question how CST can reduce monocyte and granulocyte infiltration in inflamed tissues such as the liver (diet induced obese mice), intestine (colitis model), heart (hypertension model) and atheromatous plaques (atherosclerosis model) (4,7,8,12,13).

To address how CST affects macrophage chemotaxis to inflamed tissues, we used the aortic ring vessel model (17) (Fig. 2A), which is based on the co-embedding of part of the aorta of $Cx_3cr1^{+/gfp}$ transgenic mice adjacent to isolated pancreatic islets (20). These islets secrete chemokines, such as vascular endothelial growth factor (VEGF)-A, resulting in the directional macrophage migration from the aortic ring as well as vessel growth towards the pancreatic islets. Migration of CX_3CR1^{+} macrophages from the aortic ring was visualized by fluorescence microscopy (19) (Fig. 2B, S2). As expected, the CX_3CR1-macrophages moved towards the pancreatic islets in absence of CST (Fig 2B). However, perfusing the aortic ring with CST (5 µM) resulted in a lower number of CX_3CR1^{+GFP} macrophages migrating towards the pancreatic islets (Fig 2B), indicating that CST blocked directional migration. Interestingly, we also observed that CST is pro-angiogenic, as it increased both

the amount and length of the sprouts and branches emanating from the aortic rings (Fig. 2C-D, S3).

The loss of directional cell migration to the pancreatic islets might be caused by blockage of chemokine-induced cell migration by CST. To investigate this possibility, we performed intravital imaging of the cremaster muscle, but this time for CST in combination with MIP-2. This resulted in the inverse effect compared to CST or MIP-2 alone: release of attached cells from the vessel wall and reduced migration of cells into the tissue (Fig. 2E, S4), indicating that despite being weakly chemotactic, CST blocks MIP-2 elicited phagocyte recruitment. To further confirm this, we performed an *in vitro* migration assay, where human monocytes were stimulated with a gradient of CCL2 in presence of CST (Fig. 2F). Similar to our findings with the intravital imaging, CST blocked monocyte migration towards the CCL2.

Although CST counteracts the chemoattraction by inflammatory cytokines (Fig. 2G), the question remains open which receptor(s) CST utilize to exert these effects on cell migration. We speculate that this might be a G-protein coupled receptor (GPCR), since GPCRs are actively involved in leukocyte migration (21) coupled with expression of GPCRs in all cell types responsive to catestatin (e.g. monocytes (10), neutrophils (22,23), macrophages (4,7,8,12,13), endothelial (13,24) and mast cells (11)), we speculate that CST might act through this receptor type. We have not only shown how CST reduces the infiltration of monocytes and macrophages in inflamed tissues (4,7,8,12,13), but offer a possible mechanistic explanation for the correlation of CST levels with improved disease outcome in patients suffering from chronic diseases (4–6), reinforcing CST as a therapeutic target for treatment of diseases associated with chronic inflammation.

4. Author contributions

E.M.M., G.C., S.K.M. and G.v.d.B. designed the study. E.M.M, K.P., G.C. designed and performed the experiments. E.M.M. and G.v.d.B wrote the manuscript and all authors participated in discussing and editing of the manuscript.

5. Disclosure of conflict of interest

The authors declare that the research was conducted in the absence of any commercial or financial relationships that could be construed as a potential conflict of interest.

6. Funding

G.v.d.B. is funded by a Young Investigator Grant from the Human Frontier Science Program (HFSP; RGY0080/2018), and a Vidi grant from the Netherlands Organization for Scientific Research (NWO-ALW VIDI 864.14.001). G.v.d.B has received funding from the European Research Council (ERC) under the European Union's Horizon 2020 research and innovation programme (grant agreement No. 862137. S.K.M. is supported by a grant from the US Department of Veterans Affairs (I01BX000323). G.C. is supported by grants from the Swedish Research Council and the Swedish Society for Medical Research. E.M.M is supported by a short-term EMBO fellowship (EMBO7887).

7. References

1. Deshmane SL, Kremlev S, Amini S, Sawaya BE. Review Monocyte Chemoattractant

Protein-1 (MCP-1): An Overview. doi:10.1089/jir.2008.0027

2. Sugimoto MA, Sousa LP, Pinho V, Perretti M, Teixeira MM. Resolution of inflammation: What controls its onset? *Front Immunol* (2016) **7**: doi:10.3389/fimmu.2016.00160

3. Muntjewerff EM, Dunkel G, Nicolasen MJT, Mahata SK, Van Den Bogaart G. Catestatin as a Target for Treatment of Inflammatory Diseases. *Front Immunol* (2018) **9**:2199. doi:10.3389/fimmu.2018.02199

4. Muntjewerff EM, Tang K, Lutter L, Gustaf C, Nicolasen MJT, Gao H, Katkar GD, Das S, ter Beest B, Ying W, et al. Chromogranin A regulates gut permeability via the antagonistic actions of its proteolytic peptides. (2020) Available at: https://www.biorxiv.org/content/10.1101/2020.09.19.304303v1.full.pdf

5. Zivkovic PM, Matetic A, Tadin Hadjina I, Rusic D, Vilovic M, Supe-Domic D, Borovac JA, Mudnic I, Tonkic A, Bozic J. Serum Catestatin Levels and Arterial Stiffness Parameters Are Increased in Patients with Inflammatory Bowel Disease. *J Clin Med* (2020) **9**:628. doi:10.3390/jcm9030628

6. Corti A, Marcucci F, Bachetti T. Circulating chromogranin A and its fragments as diagnostic and prognostic disease markers. *Pflügers Arch - Eur J Physiol* (2017) **470**:199–210. doi:10.1007/s00424-017-2030-y

7. Ying W, Mahata S, Bandyopadhyay GK, Zhou Z, Wollam J, Vu J, Mayoral R, Chi N-W, Webster NJG, Corti A, et al. Catestatin Inhibits Obesity-Induced Macrophage Infiltration and Inflammation in the Liver and Suppresses Hepatic Glucose Production, Leading to Improved Insulin Sensitivity. *Diabetes* (2018) **67**:841–848. doi:10.2337/db17-0788

8. Rabbi MF, Labis B, Metz-Boutigue MH, Bernstein CN, Ghia J-E. Catestatin decreases macrophage function in two mouse models of experimental colitis. *Biochem Pharmacol* (2014) **89**:386–398. doi:10.1016/j.bcp.2014.03.003

9. Mahapatra NR, O'Connor DT, Vaingankar SM, Hikim APS, Mahata M, Ray S, Staite E, Wu H, Gu Y, Dalton N, et al. Hypertension from targeted ablation of chromogranin A can be rescued by the human ortholog. *J Clin Invest* (2005) **115**:1942–1952. doi:10.1172/jci24354

10. Egger M, Beer AGE, Theurl M, Schgoer W, Hotter B, Tatarczyk T, Vasiljevic D, Frauscher S, Marksteiner J, Patsch JR, et al. Monocyte migration: A novel effect and signaling pathways of catestatin. *Eur J Pharmacol* (2008) **598**:104–111. doi:10.1016/j.ejphar.2008.09.016

11. Aung G, Niyonsaba F, Ushio H, Kajiwara N, Saito H, Ikeda S, Ogawa H, Okumura K. Catestatin, a neuroendocrine antimicrobial peptide, induces human mast cell migration, degranulation and production of cytokines and chemokines. *Immunology* (2011) **132**:527–539. doi:10.1111/j.1365-2567.2010.03395.x

12. Ying W, Tang K, Avolio E, Schilling JM, Pasqua T, Liu MA, Cheng H, Zhang J, Mahata S, Bandyopadhyay G, et al. Catestatin (CST) is a key mediator of the immunoendocrine regulation of cardiovescular function. (2020) Available at:

https://doi.org/10.1101/2020.05.12.092254

13. Kojima M, Ozawa N, Mori Y, Takahashi Y, Watanabe-Kominato K, Shirai R, Watanabe R, Sato K, Matsuyama T, Ishibashi-Ueda H, et al. Catestatin Prevents Macrophage-Driven Atherosclerosis but Not Arterial Injury–Induced Neointimal Hyperplasia. *Thromb Haemost* (2018) **118**:182–194. doi:10.1160/TH17-05-0349

14. Jung S, Aliberti J, Graemmel P, Sunshine MJ, Kreutzberg GW, Sher A, Littman DR. Analysis of Fractalkine Receptor CX3CR1 Function by Targeted Deletion and Green Fluorescent Protein Reporter Gene Insertion. *Mol Cell Biol* (2000) **20**:4106–4114. doi:10.1128/mcb.20.11.4106-4114.2000

15. Baranov MV, Bianchi F, Schirmacher A, van Aart MAC, Maassen S, Muntjewerff EM, Dingjan I, ter Beest M, Verdoes M, Keyser SGL, et al. The Phosphoinositide Kinase PIKfyve Promotes Cathepsin-S-Mediated Major Histocompatibility Complex Class II Antigen Presentation. *iScience* (2019) **11**: doi:10.1016/j.isci.2018.12.015

16. Massena S, Christoffersson G, Hjertström E, Zcharia E, Vlodavsky I, Ausmees N, Rolny C, Li J-P, Phillipson M. A chemotactic gradient sequestered on endothelial heparan sulfate induces directional intraluminal crawling of neutrophils. *Blood* (2010) **116**:1924–1931. doi:10.1182/blood-2010-01-266072

17. Baker M, Robinson SD, Lechertier T, Barber PR, Tavora B, D'Amico G, Jones DT, Vojnovic B, Hodivala-Dilke K. Use of the mouse aortic ring assay to study angiogenesis. *Nat Protoc* (2012) **7**:89–104. doi:10.1038/nprot.2011.435

18. Bohman S, Andersson A, King A. No differences in efficacy between noncultured and cultured islets in reducing hyperglycemia in a nonvascularized islet graft model. *Diabetes Technol Ther* (2006) **8**:536–545. doi:10.1089/dia.2006.8.536

19. Schindelin J, Arganda-Carreras I, Frise E, Kaynig V, Longair M, Pietzsch T, Preibisch S, Rueden C, Saalfeld S, Schmid B, et al. Fiji: An open-source platform for biological-image analysis. *Nat Methods* (2012) **9**:676–682. doi:10.1038/nmeth.2019

20. Nicosia RF, Gelati M, Aplin AC, Fogel E, Smith KD. Macrophages Requires Injury and Inflammatory Cytokines The Angiogenic Response of the Aorta to. *J Immunol Ref* (2008) **181**:5711–5719. doi:10.4049/jimmunol.181.8.5711

21. Lämmermann T, Kastenmüller W. Concepts of GPCR-controlled navigation in the immune system. *Immunol Rev* (2019) **289**:205–231. doi:10.1111/imr.12752

22. Zhang D, Shooshtarizadeh P, Laventie BJ, Colin DA, Chich JF, Vidic J, de Barry J, Chasserot-Golaz S, Delalande F, Van Dorsselaer A, et al. Two chromogranin a-derived peptides induce calcium entry in human neutrophils by calmodulin-regulated calcium independent phospholipase A2. *PLoS One* (2009) **4**:e4501. doi:10.1371/journal.pone.0004501

23. Briolat J, Wu SD, Mahata SK, Gonthier B, Bagnard D, Chasserot-Golaz S, Helle KB, Aunis D, Metz-Boutigue MH. New antimicrobial activity for the catecholamine release-inhibitory peptide from chromogranin A. *Cell Mol Life Sci* (2005) **62**:377–385. doi:10.1007/s00018-004-4461-9

24. Theurl M, Schgoer W, Albrecht K, Jeschke J, Egger M, Beer AGE, Vasiljevic D, Rong S, Wolf AM, Bahlmann FH, et al. The Neuropeptide Catestatin Acts As a Novel Angiogenic Cytokine via a Basic Fibroblast Growth Factor-Dependent Mechanism. *Circ Res* (2010) **107**:1326–1335. doi:10.1161/circresaha.110.219493

8. Figure legends

Fig. 1: CST is weakly chemotactic. (A) Scheme showing set-up of Gradientech migration assay. Two syringes filled with buffer +/- chemoattractant were connected to the device (green) to create a flow (*x*-direction) and perpendicular (*y*) cytokine gradient. The inset shows migration of monocytes along the flow and towards the chemoattractant. **(B)** Representative tracks of human monocytes showing the *x*- and *y*-movement of individual cells upon exposure to the indicated buffer, 5 µM CST or 0.5 nM CCL2. **(C)** Quantification of panel B (N=3). **(D)** Scheme showing set-up of cremaster muscle imaging in mice to visualize phagocyte (monocytes and granulocytes) extravasation *in vivo*. **(E)** Phagocyte rolling velocity (top) and attachment (bottom) upon overflowing the muscle with buffer (control, gray), 0.5 nM MIP-2 (blue) or 5 µM CST (black) (N=3, two-way ANOVA). **(F)** Representative images of granulocyte attachment as visualized by Ly6G-mAb (green) to the vessel wall upon only buffer, MIP-2 or CST stimulation. *: P<0.05; **: P<0.01; ***P<0.001; ns: not significant.

Fig. 2: CST blocks migration induced by inflammatory chemokines and promotes angiogenesis. (A) Scheme showing set-up of aortic ring assay. Aortic ring was isolated from CX_3CR1-GFP mice and embedded adjacent to pancreatic islets in collagen I. Image shows islets (blue), CD31 (red) and CX_3CR1 (green). **(B)** Representative images of CX3CR1-macrophage migration upon control or CST stimulation of the aortic ring. The graph shows the percentage of cells above (yellow) the center of mass (N=8). **(C)** Representative images of vessels by CD31 (red) upon control or CST stimulation of the aortic ring. **(D)** Quantification of angiogenesis. Total number of sprouts and branches (left) and their length (right) (N=5-6). **(E)** Cremaster muscle imaging. Phagocyte attachment to vessel wall upon overflowing the muscle with buffer (control, gray) and buffer with the chemoattractant MIP-2 (blue), CST (black) or both (red) (N=3, two-way ANOVA). **(F)** Gradientech migration assay. Representative *x*- and *y*-movement of human monocytes exposed to opposite gradients of CST and CCL2 (N=3). **(G)** Model showing leukocyte extravasation in presence of low and high concentrations of CST. Mann-Whitney test *: P<0.05; **: P<0.01; ***P<0.001; ****P<0.0001; ns: not significant.

Sup. 1: Attachment of granulocytes and monocytes to vessel wall. (A) Venules of the cremaster muscle were overflown with bicarbonate-buffered saline buffer (buffer only control), the chemoattractant MIP-2 or CST as shown in main Fig. 1D-F. Graph shows quantification of rolling cells (cells/min). **(B)** Quantification of cell in tissue. **(C)** Representative brightfield snapshots of *in vivo* cremaster muscle imaging as in main figure 1D-F. **(C)** Quantification of adherent granulocytes (visualized by Ly6G-mAb, main Fig. 1F) and monocytes (brightfield, panel C) after 0, 30, 60 and 90 minutes (N=1-2).

Sup. 2: Quantification of CX3XR1+ cell movement in the aortic ring model. (A) Brightfield image of the aortic ring with islets. **(B)** Description of CX3CR1-cell movement quantification by determination of total amount outside the aortic ring (endothelium), center of mass (red spot) and the islet side (black arrow).

Sup. 3: Branches and sprouts in the aortic ring assay. (A) Representative images of angiogenesis quantification of main figure 2C-D. The images show the ring endothelium, main sprout (red), branch (gray) **(B)** Quantification of total number of sprouts and branches separately and their length (N=5-6). Mann-Whitney test *: P<0.05; ***P<0.001; ns: not significant.

Sup. 4: The combination of CST and MIP-2 reduced chemotaxis. Venules of the cremaster muscle were overflown with bicarbonate-buffered saline buffer (buffer only control), the chemoattractant MIP-2 or CST, as shown in main Fig. 1D. Graph shows quantification of tissue migration **(A)**, rolling cells (cells/min) **(B)** and velocity **(C)** upon CST, MIP-2 or stimulation with both (N=3, two-way ANOVA) *: P<0.05; **: P<0.01; ***P<0.001; ****P<0.0001; ns: not significant.

9. Figures

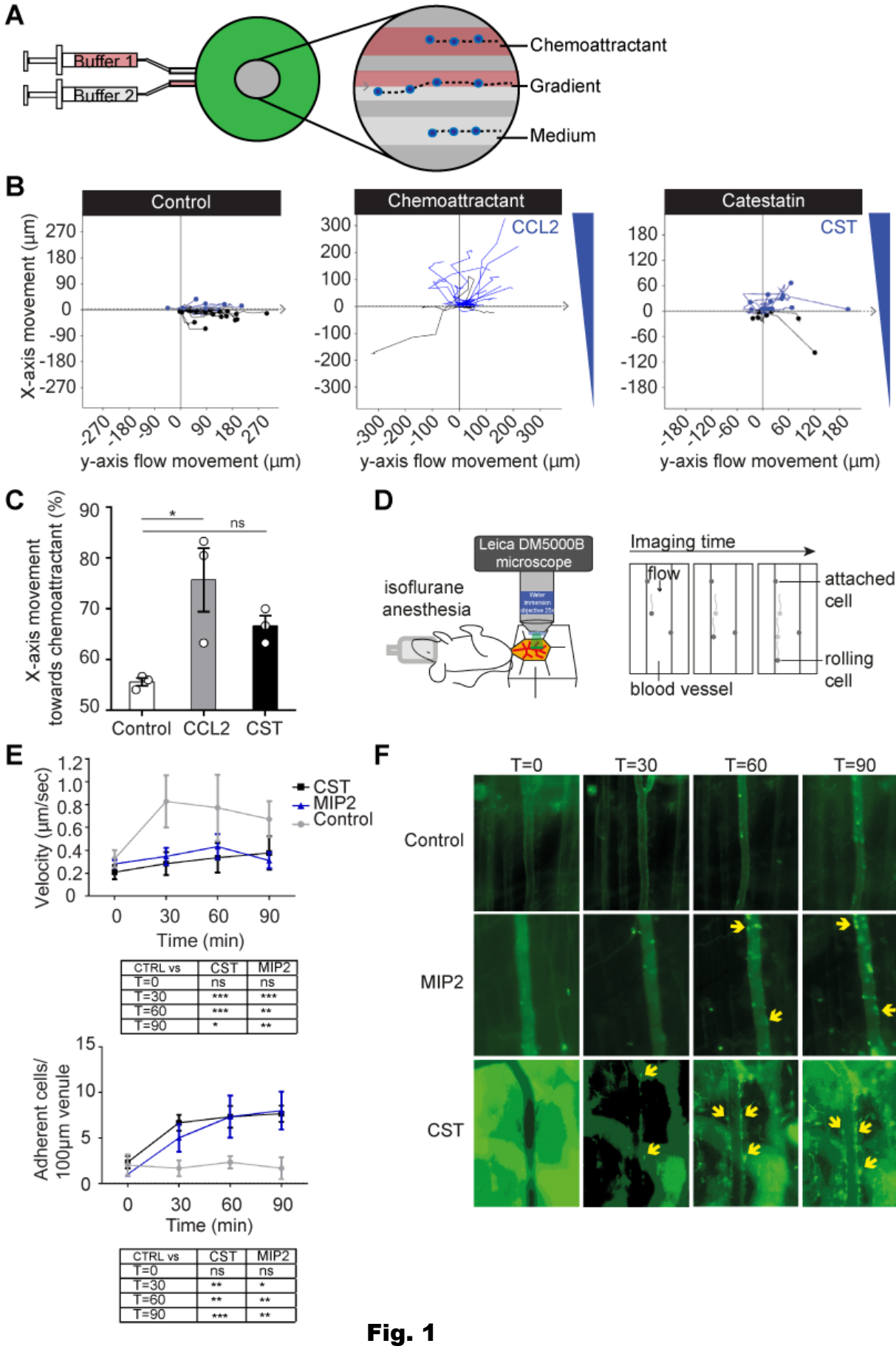

Fig. 1

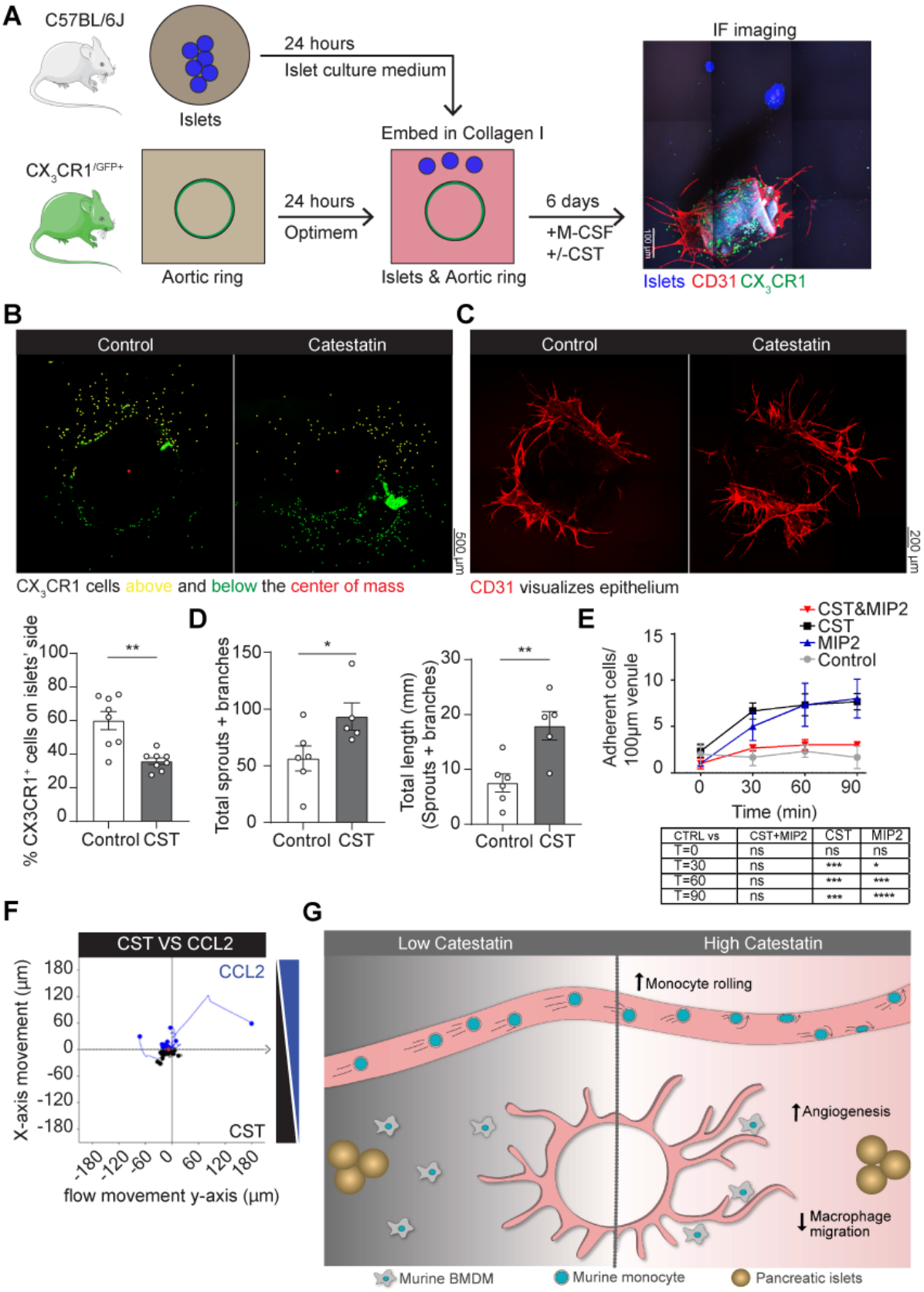

Fig. 2